

Influence of Process Parameters on the Mechanical Behavior of an Ultrafine-Grained Al Alloy

TROY D. TOPPING, BYUNGMIN AHN, YING LI, STEVEN R. NUTT,
and ENRIQUE J. LAVERNIA

Aluminum alloys with nanocrystalline (NC) and ultrafine grain (UFG) size are of interest because of their strengths that are typically 30 pct greater than conventionally processed alloys of the same composition. In this study, UFG AA 5083 plate was prepared by quasi-isostatic (QI) forging of cryomilled powder, and the microstructure and mechanical behavior was investigated and compared with the behavior of coarse-grained AA 5083. Forging parameters were adjusted in an effort to strengthen the UFG material while retaining some tensile ductility. Different forging parameters were employed on three plates, with approximate dimensions of 254 mm diameter and 19 mm thickness. The overarching goal of the current effort was to increase strength through minimized grain growth during processing while maintaining ductility by breaking up prior particle boundaries (PPBs) with high forging pressures. Mechanical tests revealed that strength increased inversely with grain size, whereas ductility for some of the experimental materials was preserved at the level of the conventional alloy. The application of the Hall-Petch relationship to the materials was studied and is discussed in detail with consideration given to strengthening mechanisms other than grain size, including dispersion (Orowan), solid solution, and dislocation strengthening.

DOI: 10.1007/s11661-011-0849-y

© The Minerals, Metals & Materials Society and ASM International 2011

I. INTRODUCTION

BALL milling of metal powders in cryogenic media (cryomilling), such as liquid nitrogen (LN₂) or liquid argon, can be used to produce large quantities (*e.g.*, 1 to 35-kg batches) of nanocrystalline (NC) microstructures in relatively short times.^[1,2] Milling time is reduced compared with conventional ball-milling partly because of the inhibition of recovery at cryogenic temperatures [approximately 77 K to 84 K (−196 °C to −189 °C)].^[3] However, subsequent consolidation and processing of cryomilled powders and forming of compacts to produce bulk samples typically involves high temperatures, which often causes grain growth.^[4] Thermal exposure can occur during hot vacuum degassing, hot isostatic pressing (HIP), quasi-isostatic (QI) forging, extrusion, and rolling, depending on the processing route chosen.

In this study, an Al-Mg alloy (AA 5083) was investigated because of its high specific strength, thermal stability, and resistance to corrosion. These attributes are important for applications in both civilian and military vehicles, and this research focused particularly on developing lightweight armor applications for future

amphibious assault vehicles.^[5] Liquid nitrogen (LN₂) was used as a cryomilling medium for the following reasons. First, the low temperature during milling inhibits recovery and dynamic recrystallization; second, the incorporation of nitrogen into the matrix microstructure enhances mechanical properties; and third, the liquid nitrogen environment limits oxygen contamination from the atmosphere.^[2,6,7] While acknowledging the effects of the nitrogen in this system, the primary goal of this investigation was to determine the effect of grain size on strength in the alloy by controlling the processing temperatures and limiting grain growth. Subsequently, a Hall-Petch type relationship was shown for three similarly processed AA 5083 plates. To perform an accurate study of the influence of processing temperatures, the three plates considered were consolidated from the same batch of cryomilled powder. Additionally, all plates were processed via QI forging in three steps to achieve similar nominal diameters and thicknesses. QI forging was chosen over HIP and/or extrusion because it is reportedly the most effective method of the three for breaking up prior particle boundaries (PPBs), thus enhancing ductility and toughness.^[8]

After consolidation, the resulting microstructures consisted of slightly nonequiaxed ultrafine grains (100 to 500 nm). The ultra-fine grain (UFG) microstructure is desirable for the potential applications mentioned because of the combination of strength and ductility that can be achieved.^[5,9] When compared with conventional, armor-grade AA 5083 H131, the plates manufactured for this investigation demonstrate superior strength, and ductility losses scale with processing temperature. The weakest of the three plates shows

TROY D. TOPPING, PhD Candidate, YING LI, Postdoctoral Researcher, and ENRIQUE J. LAVERNIA, Distinguished Professor, are with the Department of Chemical Engineering and Materials Science, University of California, Davis, CA 95616. Contact e-mail: ttopping@ucdavis.edu BYUNGMIN AHN, Research Assistant Professor and STEVEN R. NUTT, Professor, are with the Department of Chemical Engineering and Materials Science, University of Southern California, Los Angeles, CA 90089.

Manuscript submitted February 17, 2011.

Article published online August 19, 2011

ductility similar to conventional material, although strength increases by approximately 30 pct.

The objective of this study was to determine the effects of forging parameters on the mechanical behavior of a cryomilled UFG Al alloy by producing and analyzing three similar, large production-scale plates (disks were ~20 mm thick \times ~250 mm diameter) processed at 523 K, 623 K, and 723 K (250 °C, 350 °C, and 450 °C) to control the grain size. Based on the variations in strength and microstructure for the three temperatures used, process parameters were related to strengthening mechanisms in the QI-forged, cryomilled alloy.

II. EXPERIMENTAL PROCEDURES

A. Cryomilling and Degassing

The plates used in this investigation were consolidated from cryomilled, gas-atomized -250 mesh ($<63 \mu\text{m}$) AA 5083 (Al-4.4Mg-0.7Mn-0.15Cr wt pct) powder (produced by Valimet, Inc., Stockton, CA). All cryomilled powder for the plates investigated was from the same batch, which was the second of four consecutive AA 5083 cryomilling runs. Note that second-run powder is considered production-quality powder, whereas first runs are generally classified as a “break-in” runs, which are used to coat and condition the system. Each batch started with 20-kg powder, with final yields >95 pct. Because of the scale of the project, cryomilling was performed by a commercial vendor (DWA Aluminum Composites, Chatsworth, CA) operating under the supervision of UC Davis and Pratt & Whitney Rocketdyne, Inc. (Canoga Park, CA).

Milling was performed using a modified Szegvari attritor, which is shown in Figure 1 with a cryogenic LN_2 medium-containing, stainless steel milling balls with a 32:1 ball-to-powder weight ratio. Milling required the addition of 0.2 wt pct stearic acid (~50/50 stearic and palmitic acids) to the 20-kg powder to act as a process



Fig. 1—Cryomilling of 20-kg batch at DWA Aluminum Composites (Chatsworth, CA) using modified Szegvari attritor (courtesy of Mark van den Bergh).

control agent (PCA). The PCA reduces agglomeration and cold welding of the powders during milling, thus enhancing the yield. To remove moisture and other contamination related to the use of the PCA, the powder was hot vacuum degassed after filling three separate AA 6061 cans with approximately 3.5-kg cryomilled powder. The original outer dimensions of the cans, prior to forging, were ~19.5 cm high \times 15.2 cm diameter. Canning was performed in a glove box under flowing N_2 gas in an effort to limit exposure of the powders to atmosphere, oxygen in particular. Degassing took place over several days to reach pressures on the order of 10^{-6} torr by applying vacuum through a ~7.7-mm I.D. stem at temperatures up to 723 K (450 °C). After degassing, the can stems were crimped and welded to prevent contamination prior to forging.

B. Quasi-Isostatic Forging

After crimping and welding, the cans were QI forged by Advance Materials & Manufacturing Technologies, LLC (Granite Bay, CA) using three different preheat temperatures [523 K, 623 K, and 723 K (250 °C, 350 °C, and 450 °C)], while using a single forging load (22.24 MN) during the initial forgings. The soak times prior to forging were also varied for each temperature in an effort to limit grain growth. After heating, the cans were placed in the die, surrounded by a bed of preheated pressure transmission medium, which is shown schematically in Figure 2. The cans were then forged at nominally slow velocities—on the order of 1 mm/s—until the desired load was reached. All three can heights

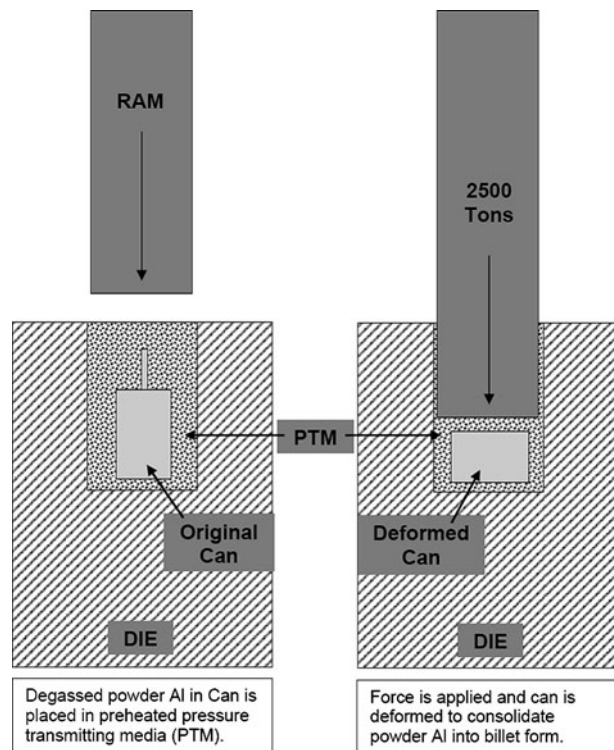


Fig. 2—Schematic of QI forging at Advance Materials & Manufacturing Technologies (AM2T).

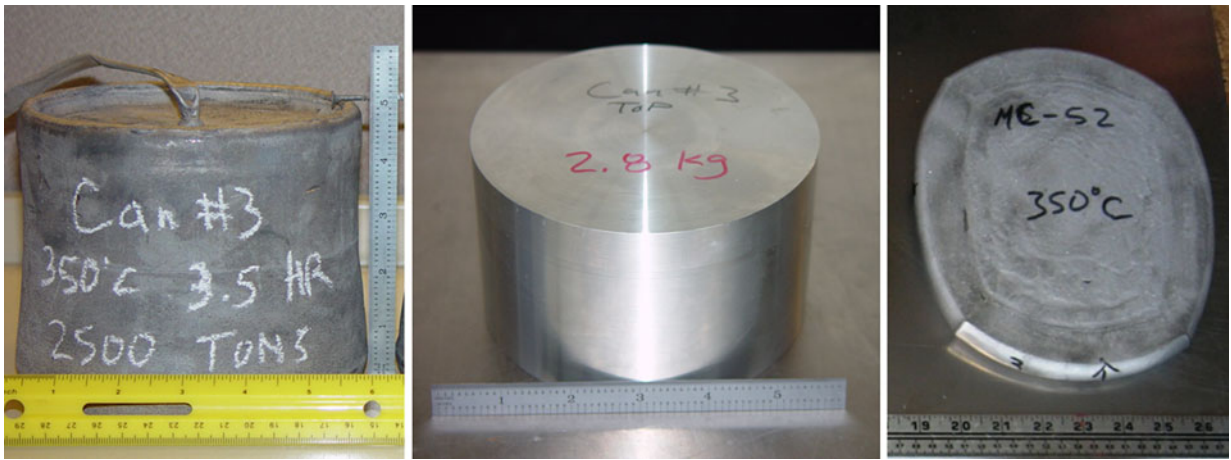


Fig. 3—Plate forged at 623 K (350 °C) after one forging, before and after removal of outer can (left and center), and in the final geometry after three forgings (right).

deformed approximately 35 pct during the first forging. After the first set of forgings, the outer can material was removed by machining on a lathe to reveal the fully dense cylindrical billets of consolidated AA 5083 powder. Two subsequent forgings were conducted for each of the three plates, continuing the use of three different soak temperatures. Figure 3 shows one plate after one forging and in the final geometry. These forgings were displacement controlled, as opposed to load controlled, to achieve the desired final plate thicknesses of ~20 mm.

C. Standard Commercial Plate

A rectangular section of conventionally processed “armor-grade” AA 5083 H131 plate, 19.0 mm transverse thickness, was used for comparison with the cryomilled plates. Because of the commercial origin of this plate, it was most likely produced by ingot casting followed by hot rolling, then cold worked to achieve the H131 condition. The plate was assumed to have primary and secondary/normal rolling directions parallel to the length and width, respectively. The H131 temper refers to the rolling conditions and degree of cold work imparted to the plate. The number 1 indicates cold rolled and the number 3 indicates the strength increase on a scale of 1 to 9. The last number 1, of the 131 temper, refers to any specific variation in the temper from the first two numbers. The last number in the temper could be a proprietary treatment peculiar to the metal forming mill.^[10]

D. Microstructural Characterization

The concentration of metallic alloying elements was measured using direct current plasma emission spectroscopy according to ASTM E 1097-03 by Luvak, Inc. (Boylston, MA). Two vendors were used to measure the concentration of nonmetallic elements in the plates (H, O, N, and C). Initially, only the plate forged at 723 K (450 °C) was sent for analysis because all powder for the plates came from the same cryomilling batch. However,

because the hot vacuum degassing was performed separately, specimens from each plate were also sent to a second vendor, serving to verify degassing consistency and accuracy of data from the two chemical analysis vendors. The first vendor, LECO, Corp. (St. Joseph, MI), measured concentrations in the plate forged at 723 K (450 °C) using inert gas fusion analyzers for H (RH-404), and for O and N (TCH-600), and combustion combined with IR detection for C (CS-600). The second vendor, ATI Wah Chang (Albany, OR), measured concentrations in all three plates using inert gas fusion analyzers for H (RH404), and for O and N (TC-436), and combustion combined with IR detection for C (CS-444). ATI Wah Chang also verified the N concentrations via the Kjeldahl distillation method.^[11]

Density measurements were performed using an Ar gas displacement pycnometer (AccuPyc-1330; Micromeritics, Atlanta, GA) with a 3.5-cm³ chamber, at least 80 pct of which was filled by the samples. Five sets of 20 measurements were made for each material, achieving an accuracy of ±0.001 g/cm³.

Metallographic polishing was performed on samples of plates sectioned in different orientations with respect to the extrusion, forging, or rolling directions, for examination in an optical microscope (Olympus AHMT3; Olympus, Center Valley, PA). Image analysis was performed to measure the fraction of coarse-grained regions using software (Adobe Photoshop; Adobe, San Jose, CA, and Fovea Pro; Reindeer Graphics, Asheville, NC). For the micrographs, the materials were sectioned with two different processing orientations (parallel and transverse to forging direction). The prepared specimens were fine polished and chemically etched with detergent to emphasize coarse-grained regions, which seemed lighter than the UFG matrix.

Slices of material were thinned for transmission electron microscope (TEM) examination (Philips EM420T, Mahwah, NJ) by jet polishing in ethanol containing 8 pct perchloric acid and 10 pct 2-butoxyethanol. The maximum dimensions of 400 individual grains were measured from TEM images, generating a grain size histogram, from which the number-based, mean grain size, and aspect ratio

were obtained. The mean grain size and aspect ratio of the standard plate, etched with Keller's reagent (water containing 2.5 pct nitric acid, 1.5 pct hydrochloric acid, and 1 pct hydrofluoric acid), was obtained from micrographs using a 10-line intercept method.^[12]

The grain orientation was characterized for the conventionally processed standard AA 5083 plate and the plate cryomilled and forged at 523 K (250 °C) by electron backscattered diffraction (EBSD) with a field-emission scanning electron microscope (FESEM; JEOL JSM-7001F; JEOL Ltd., Tokyo, Japan). The EBSD specimens were prepared using a broad ion beam cross-section polisher (JEOL, SM-09010) using a low-voltage (5 kV) Ar ion beam. A high-speed detector (Hikari, EDAX-TSL, Mahwah, NJ) was used for EBSD pattern acquisition at an acceleration voltage of 10 kV and a working distance of 15 mm. The data were analyzed using the OIM software (EDAX-TSL). Raw data underwent standard cleaning procedures, such as the confidence index standardization (CI < 0.1) and the grain dilation method with a single iteration.

Additional TEM specimens were prepared at University of California–Davis by sectioning the bulk materials, mechanical grinding to a thickness <30 μm, then dimpling (VCR D500i dimpler) to approximately 20 μm from two sides of the sample. Subsequent thinning to a thickness of electron transparency was carried out using a Gatan precision ion polishing system 691 with Ar and an accelerating voltage of 4 kV. High-resolution TEM (HRTEM) was performed on a JEOL JEM 2500 SE transmission electron microscope with an operating voltage of 200 kV. Fast Fourier transformed (FFT) images were used to quantify dislocation densities in the plate forged at 523 K (250 °C) before and after annealing for 15 minutes at 688 K (415 °C). The image area was correlated to the dislocation density per unit area with the understanding that one third of the dislocations are not visible in the two-beam condition.

E. Mechanical Behavior

The tensile behavior in the plane of the plates was measured using flat dog-bone specimens approximating to subsize ASTM E 8M^[13] (with nominal gauge sections 40 × 6 × 3 mm). The specimens were deformed at a strain rate of 10⁻³/s using a universal testing machine (Instron 8801), with strain measured by a standard video extensometer. The presented tensile property data, which were derived from the resultant stress–strain curves, represent a mean from two measurements unless stated otherwise. Vickers microhardness tests were performed using a microhardness tester (Buehler Micromet 2004) with a 100-g load and 15-second load time to verify the property trends in the three forged plates. Nine microhardness tests were performed on each specimen.

III. RESULTS

A. Microstructure

Microstructural variations of three plates forged at different temperatures, which was described in Table I,

Table I. Chemical Analysis and Density Measurements for Three Forged Plates

Forged Sample [K (°C)]	Density (g/cm ³)	Al (wt pct)	Mg (wt pct)	Mn (wt pct)	Cr (wt pct)	Fe (wt pct)	O (wt pct)	C (wt pct)	N (wt pct)	N* (wt pct)	H (ppm)
523 (250)	2.6729 ± 0.0006	93.5	4.53	0.69	0.14	0.21	0.33	0.15	0.49	0.49	9
623 (350)	2.6739 ± 0.0005	93.5	4.53	0.69	0.14	0.21	0.36	0.15	0.50	0.49	10
723 (450)	2.6737 ± 0.0005	93.5	4.53	0.69	0.14	0.21	0.37	0.15	0.51	0.49	12

*The second N value is via Kjeldahl distillation method.

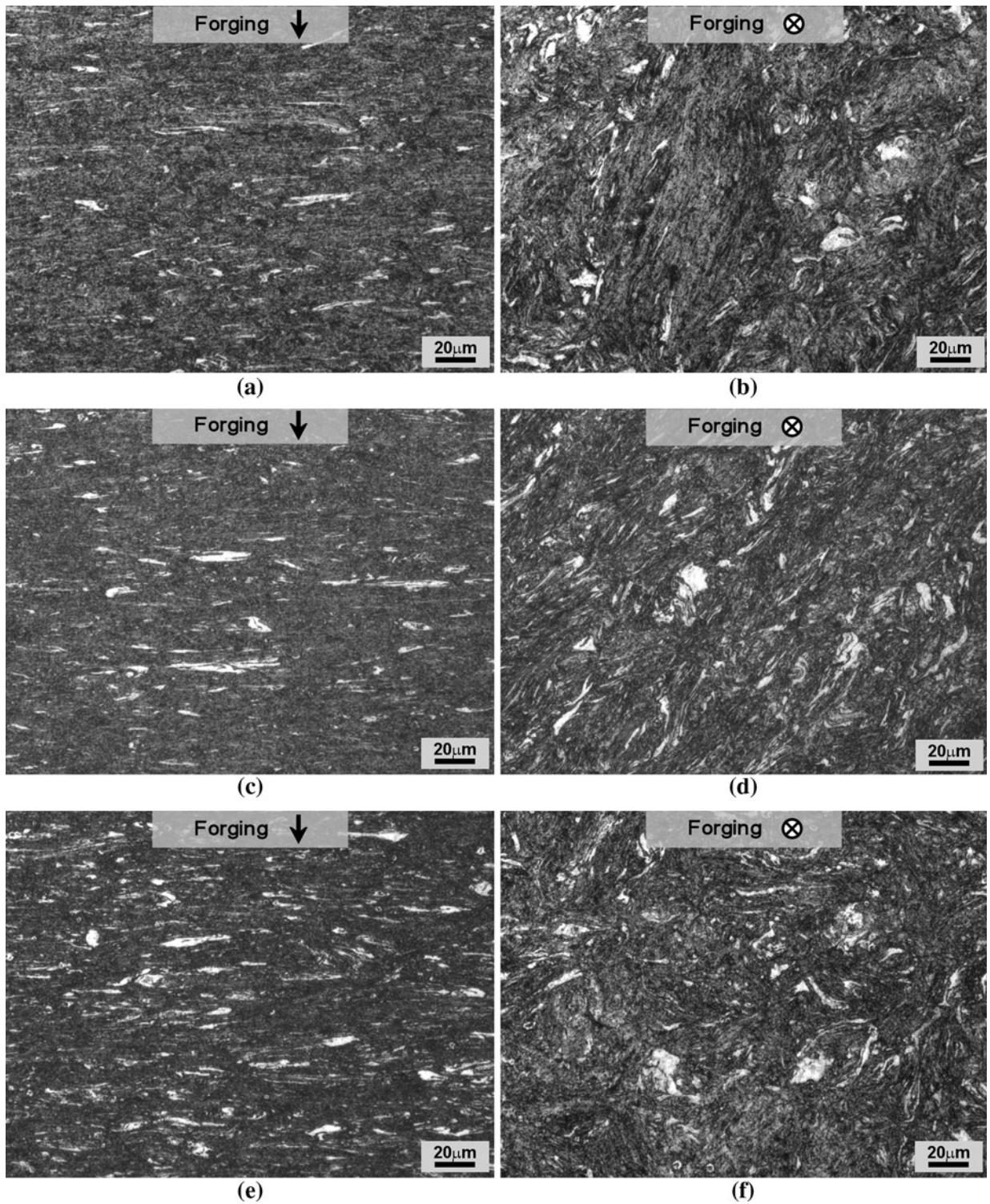


Fig. 4—Optical micrographs of chemically etched forged materials viewed in two processing directions: (a) and (b) forged at 523 K (250 °C); (c) and (d) forged at 623 K (350 °C); (e) and (f) forged at 723 K (450 °C).

were investigated using density measurements and a light microscope (Figure 4).

The metallic elements were analyzed by Luvak, Inc., whereas the interstitial data are from ATI Wah Chang Measurements. Two nitrogen values are provided,

whereas the second was obtained by an alternative method (Kjeldahl).

Table I shows the density of these materials measured by pycnometry. All materials exhibited higher density ($\sim 2.67 \text{ g/cm}^3$) than a standard AA 5083 alloy (2.66 g/cm^3),

and the optical variations between these materials were undetectable. The increase in density is likely associated with the presence of O and N in the form of oxides and nitrides in the material, which is not typical in conventional AA 5083.^[6] Also included in Table I are the chemical analysis results for the three plates (Luvak, Inc. and ATI Wah Chang). The measurements from LECO, Corp. were performed only on the forged at 723 K (450 °C), and the values for O, C, N, and H differed from those in the ATI Wah Chang report by <0.5 pct. For simplicity, the LECO results are not included in the table.

Figure 4 shows micrographs of the plates labeled according to the respective forging temperatures. No significant variations of microstructure were observed between the materials. Because the three plates analyzed in this study were all forged at the same load, the micrographs show they retain a slight vestige of PPBs. Nevertheless, most of particle boundaries have been removed. In terms of the fraction of coarse-grained regions, according to a simple image analysis, all

materials contain similar amounts of light contrast areas, corresponding to the coarse-grained regions with fraction of 5 to 8 pct.

Grain size observations and measurements were performed on the plates normal to the forging axes, as shown in Figures 5 through 7. Aspect ratios for each plate were less than two, and representative TEM micrographs revealed that the aspect ratio was even lower when observed parallel to the forging direction. Observations normal to the forging direction were analyzed to correspond to the orientation and geometry of tensile test coupons. Because of the random nature of TEM viewing orientations, however, some uncertainty remains in the orientation of the tensile coupons relative to the aspect ratios reported. Nevertheless, a trend in grain size vs forging temperature is witnessed in the plates—with sizes in the UFG regions exhibiting averaged diameters of 194, 259, and 337 nm at 523 K, 623 K, and 723 K (250 °C, 350 °C, and 450 °C), respectively.

The specimens of standard AA 5083 plate and the plate cryomilled and forged at 523 K (250 °C),

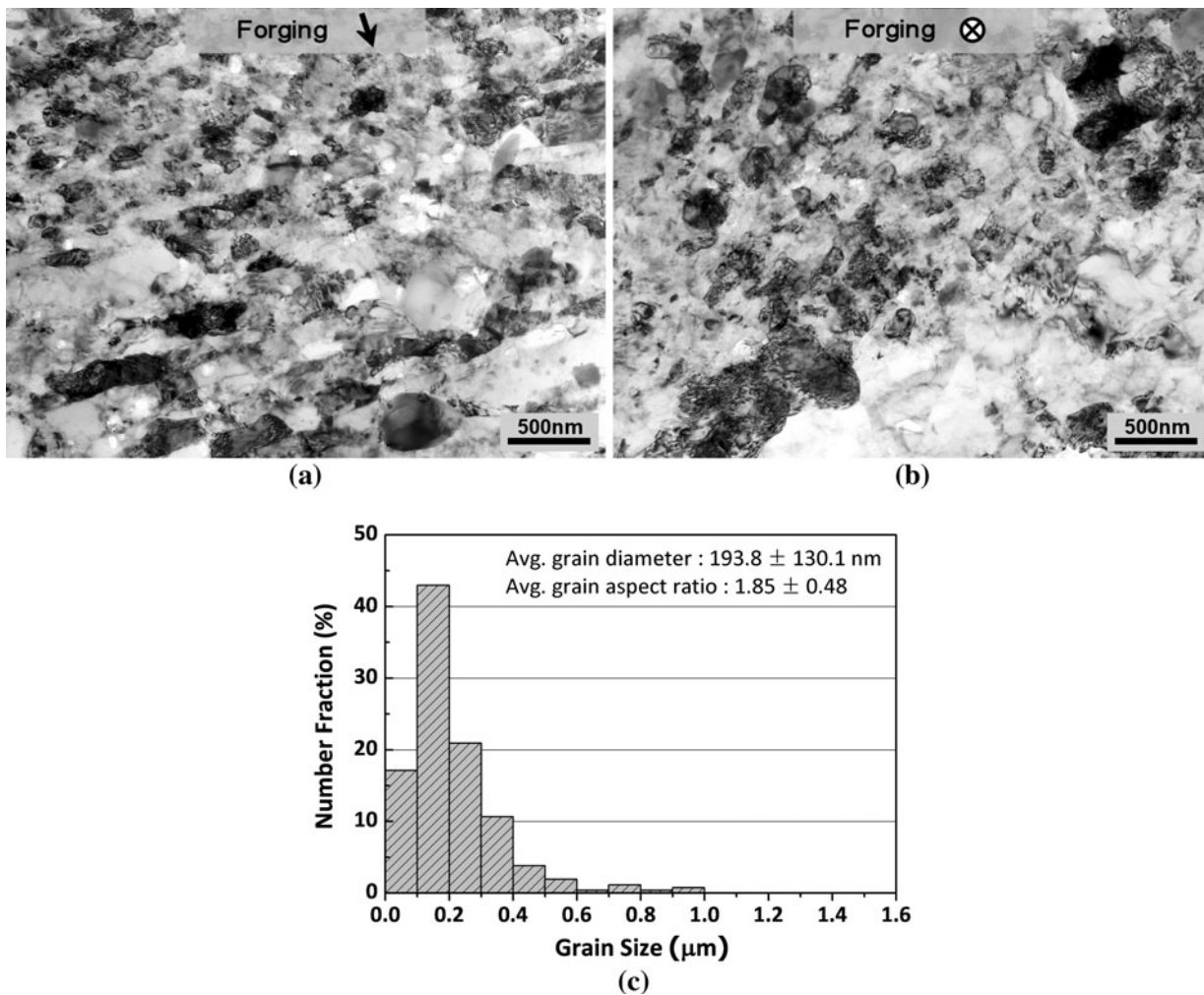


Fig. 5—Representative TEM micrographs of plate forged at 523 K (250 °C) viewed (a) normal to the forging direction and (b) in the forging direction with (c) grain size histogram.

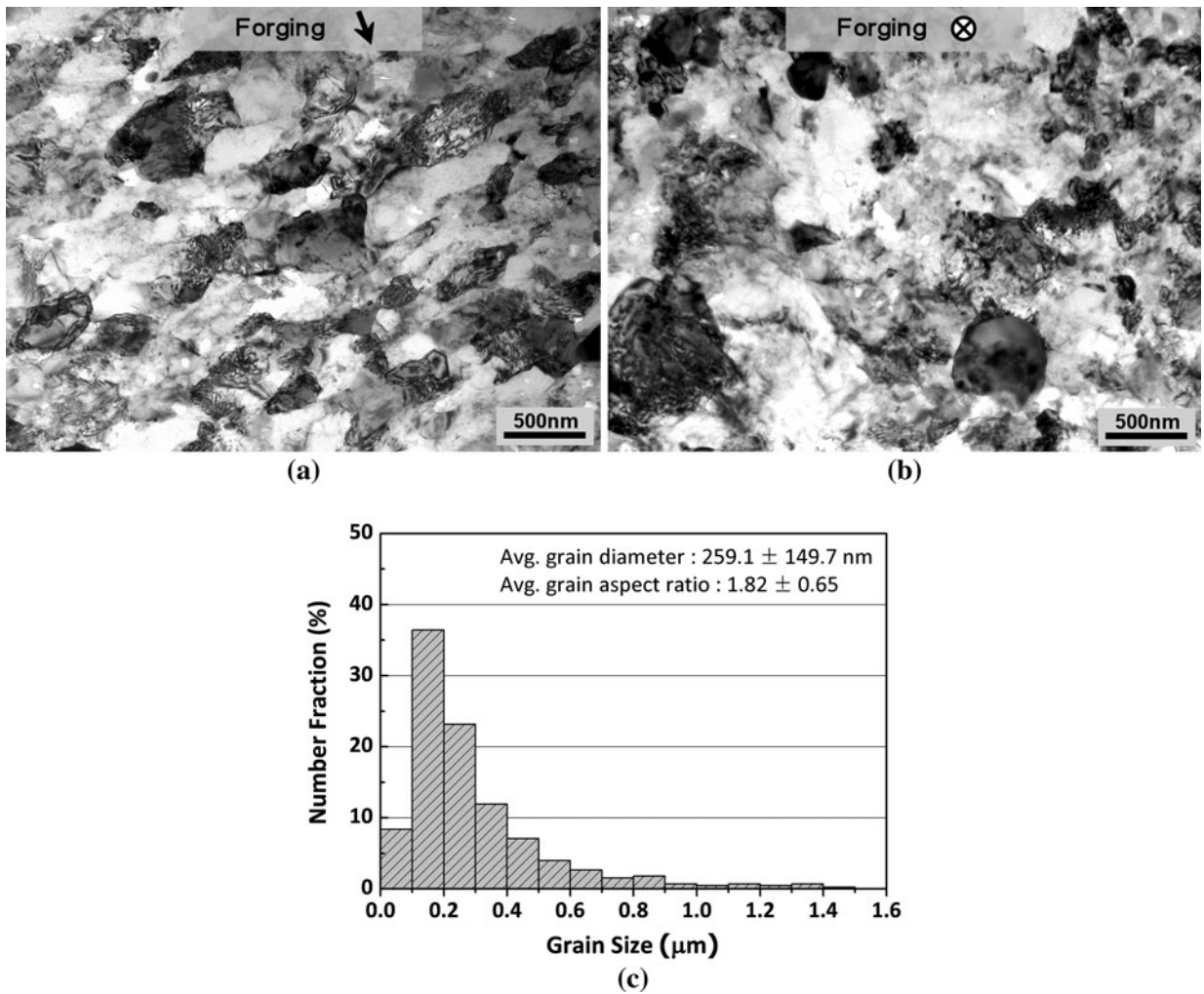


Fig. 6—Representative TEM micrographs of plate forged at 623 K (350 °C) viewed (a) normal to the forging direction and (b) in the forging direction with (c) grain size histogram.

characterized via EBSD, exhibited differences in grain boundary orientation that contribute to variations in mechanical behavior addressed in Section IV. The results shown in Figure 8 indicate a greater proportion of high-angle boundaries (HABs)—defined here as >15 deg—in the cryomilled material vs the standard plate. The standard plate contains 77 pct low-angle boundaries (LAB) and 23 pct HAB, whereas the cryomilled plate has ~65 pct HAB and 35 pct LAB. Both materials show unidentified black regions in the EBSD images, which are attributable to voids in both plates and fine grains in the cryomilled and forged plate. The black regions account for less than 1 pct of the standard plate image and ~15 pct of the cryomilled plate image. The filtered EDAX confidence index was <0.1.

B. Mechanical Behavior

A summary of mechanical properties is provided in Table II, with representative engineering stress–strain

curves plotted in Figure 9. With both Vickers hardness and tensile data shown in Table II, the mechanical property variation with forging temperature is evident. Strength, ductility, and grain size data for these plates were reported previously, without stress–strain curves and grain size histograms, in the context of studies on fatigue and fracture.^[14,15] The tensile data show expected trends of strength scaling inversely with ductility in the three plates. Stress–strain curves and property data for conventional cold-worked and annealed AA 5083 are also shown to provide a frame of reference for the impact of cryomilling on material properties after consolidation. Note that if one compares the curve for conventional H131 (cold worked) with curve for the cryomilled UFG alloy forged at 723 K (450 °C) curve, the uniform elongation is essentially the same. Strength, however, is substantially increased; yield strength increases by 39 pct, whereas ultimate strength increases by 35 pct. Other aspects of the stress–strain curves are explored in Section IV.

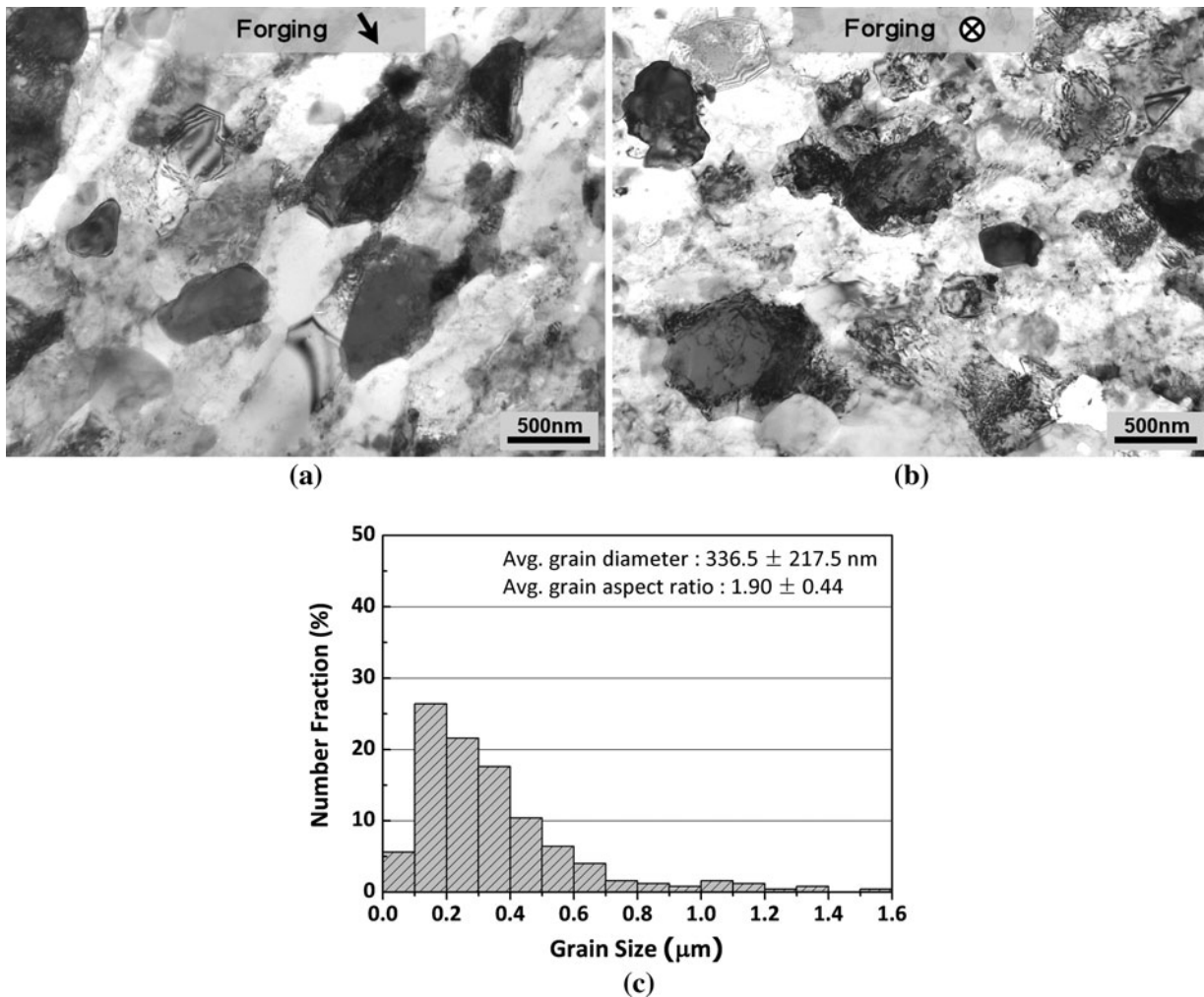


Fig. 7—Representative TEM micrographs of plate forged at 723 K (450 °C) viewed (a) normal to the forging direction and (b) in the forging direction with (c) grain size histogram.

IV. DISCUSSION

A. Strengthening Mechanisms

Strengthening in metals is attributed generally to mechanisms associated with four quantifiable characteristics of the material, such as grain size (Hall-Petch), dislocation density, solid solution alloying, and dispersion strengthening (Orowan),^[16] although recent published results obtained with NC and nanostructured metals suggest that special boundaries, such as twin boundaries, also contribute to strength.^[17–20] Although the analyses presented here focus primarily on the Hall-Petch mechanism at work, all four mechanisms contribute to the strengthening of this particular cryomilled alloy.^[6,21,22] The vast differences in grain size, grain boundary area, grain boundary orientation, and chemistry of the cryomilled *vs* conventional materials complicates a simple Hall-Petch analysis; hence, a discussion of the other three mechanisms is required, as they contribute differently in the conventional alloy *vs* the cryomilled alloys. A general equation (Eq. [1]) can be

used to represent the four hardening mechanisms, assuming that they act independently.^[17,23]

$$\sigma_{\text{Total}} = \sigma_{\text{HP}} + \sigma_{\rho} + \sigma_{\text{SS}} + \sigma_{\text{Or}} \quad [1]$$

The increase in yield strength, σ_{Total} , is a sum of the contributions of Hall-Petch, σ_{HP} , dislocation density, σ_{ρ} , solid solution, σ_{SS} , and Orowan, σ_{Or} , mechanisms.

For this analysis, we assume the solid solution mechanisms are similar in the conventional and cryomilled alloys. A few comments on this assumption are in order, and we reference work by Huskins *et al.*^[22] on conventional AA 5083 to quantify differences. Studies of similar cryomilled alloys demonstrated that magnesium goes into solution beyond the relatively low solubility limits (~1 pct) represented on the equilibrium phase diagram for Al-Mg systems.^[1,2,17] Additionally, the AA 5083 system in particular is populated with intermetallic dispersoids with compositions such as Mg_2Si , Mg_2Al_3 , $\text{Al}_{12}\text{Mg}_2\text{Cr}$, $(\text{Fe}, \text{MnCr})_3\text{SiAl}_{12}$, and $\text{Cr}_2\text{Mg}_3\text{Al}_{18}$, which can aid grain refinement and work hardening.^[1,4,8,24] Thus, not all Mg in the AA 5083 system will remain in

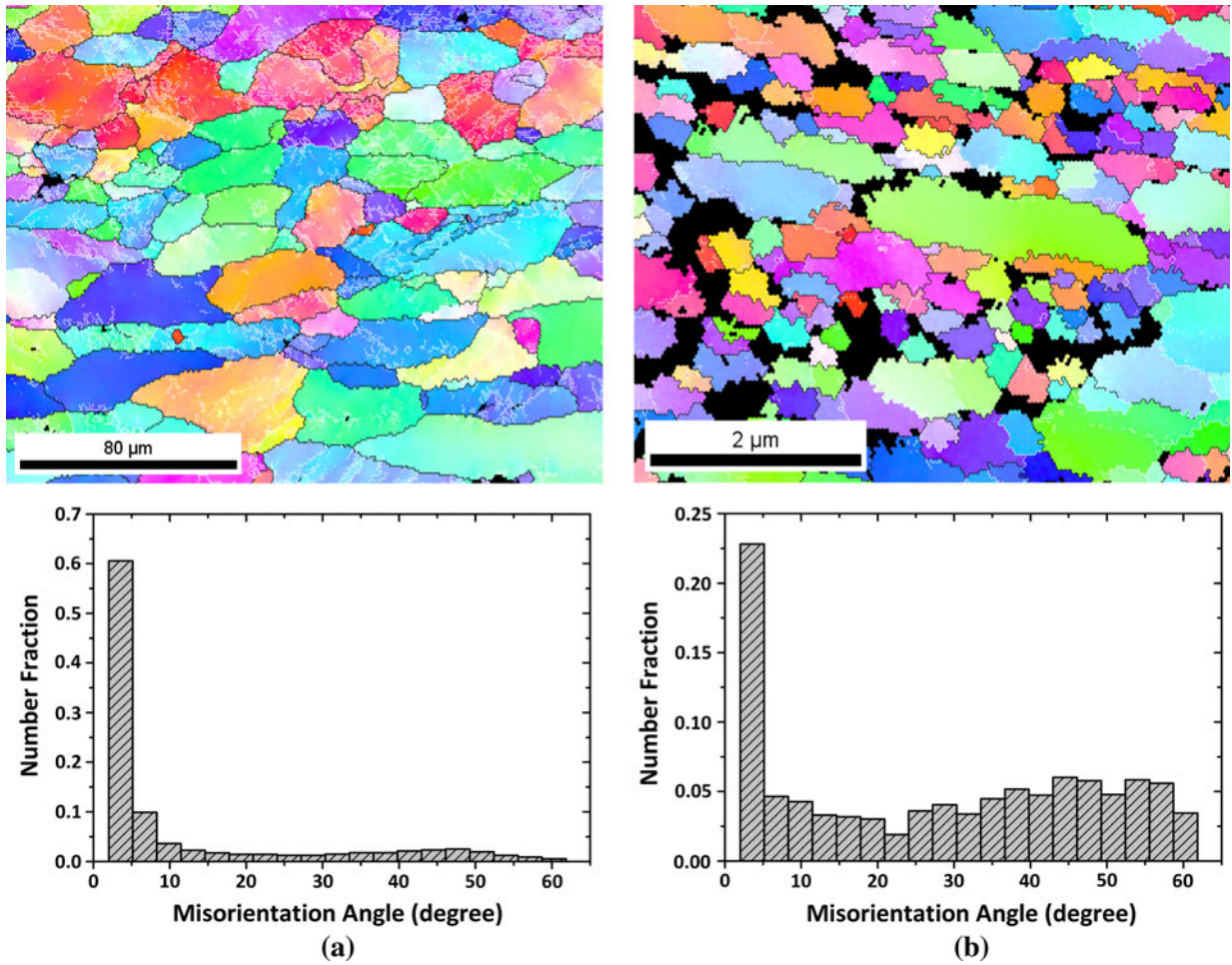


Fig. 8—EBSD images and grain boundary orientation histograms for (a) standard AA 5083 plate and (b) cryomilled plate forged at 523 K (250 °C).

Table II. Mechanical Properties for Cryomilled and Forged UFG Plates as Well as Conventional AA 5083

Material	Processing	HV (100-g load)	0.2 pct YS (MPa)	UTS (MPa)	Pct EL
UFG AA 5083	forged at 523 K (250 °C)	165 ± 3.9	521	598	3.7
	forged at 623 K (350 °C)	149 ± 8.9	451	524	6.1
	forged at 723 K (450 °C)	136 ± 5.3	400	476	10.1
Conventional AA 5083	H131 (Cold rolled)	—	287	353	10.5
	O [Annealed at 686 K (413 °C)]	—	138	308	24.8

solution. Furthermore, because one plate was processed below the recommended hot working temperatures for AA 5083 [589 K to 755 K (316 °C to 482 °C)], the possibility of dislocation hardening during forging should be considered in the analysis.^[25,26]

The grain size data presented in Figures 5 through 7 show a clear trend in grain size dependence on forging temperature. Using these data, a Hall-Petch type plot is presented in Figure 10 for the three forged plates. The Hall-Petch mechanism is well documented in the literature.^[16,27,28] In Figure 10, we simply related the yield strength to the inverse of the square of the grain size \sqrt{d}

with the initial strength being represented as the y intercept σ_o of the Eq. [2]

$$\sigma = \sigma_o + k/\sqrt{d} \quad [2]$$

The nature of the relation of σ_o to inherent frictional stress in the material is generally accepted and has been reported elsewhere.^[2,3,16,29] Using Eq. [2], the initial value of k from Figure 10 is 0.22 MPa \sqrt{m} , which is much greater than k values typically reported for pure aluminum (~ 0.07 MPa \sqrt{m}).^[29] However, a range of k values (0.09 to 0.32 MPa \sqrt{m}) has been reported for

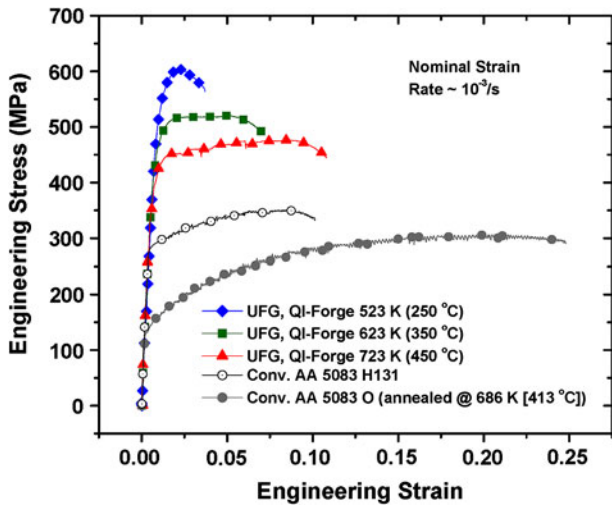


Fig. 9—Complete representative engineering stress–strain curves for three forged plates and conventional AA 5083.

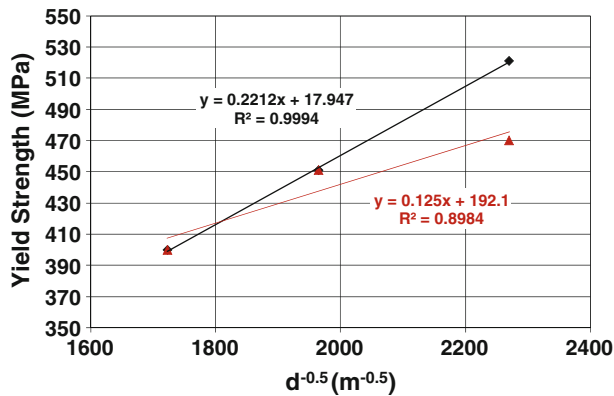


Fig. 10—Hall-Petch plot for three forged plates, before and after annealing of plate forged at 523 K (250 °C). The coefficient k is reduced from 0.22 MPa $\sqrt{\text{m}}$ to 0.125 MPa $\sqrt{\text{m}}$ by the removal of dislocation hardening.

aluminum alloys, particularly those produced by ball milling, cryomilling, and equal channel angular pressing, as summarized by Witkin and Lavernia^[2] and Hayes *et al.*^[30]

Next, we considered the possibility of work hardening during forging at 523 K (250 °C), which can lead to dislocation strengthening with multiple forging steps.^[31,32] We observed edge crack formation while forging at this temperature, which could be attributed to dislocation activity in this particular plate (no others cracked), and dislocation forests were readily visible in TEM micrographs from this material. Figure 11 shows the plate with corresponding TEM. Additionally, we performed a 15-minute anneal at 688 K (415 °C) on one of the tensile specimens following the conventional annealing treatment for AA 5083.^[26] The tensile curves for the annealed specimen, along with the as-forged specimen are shown in Figure 12, and the alternative Hall-Petch type plot is included in Figure 10. The revised k value, using the annealed specimen yield strength 470 MPa, is reduced to 0.125 MPa $\sqrt{\text{m}}$.

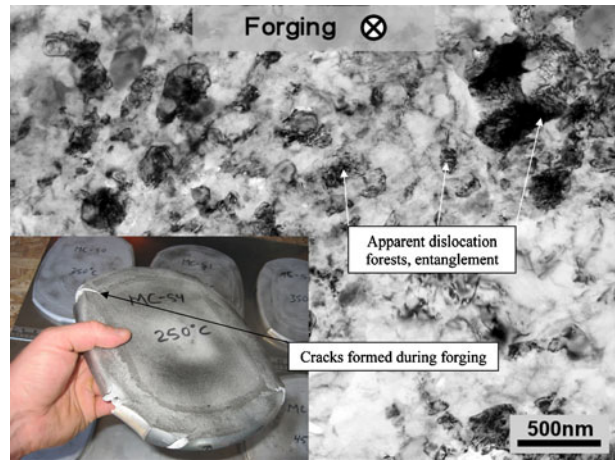


Fig. 11—TEM and macroscopic evidence reveal cold work during forging at 523 K (250 °C).

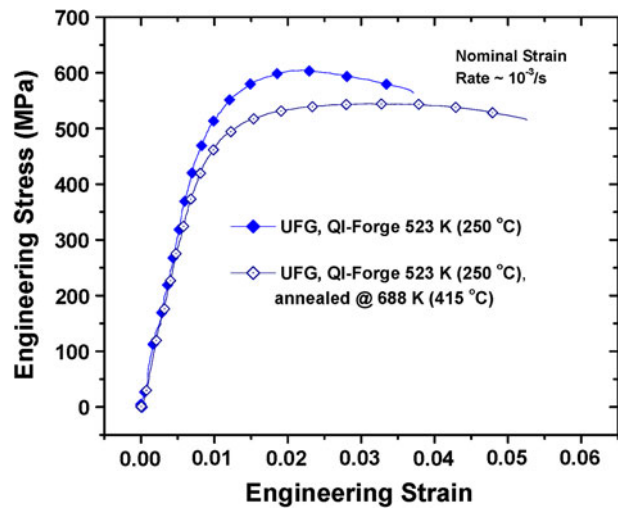


Fig. 12—Tensile stress–strain curves before and after annealing of the plate forged at 523 K (250 °C).

After reducing the effect of dislocation hardening in the plate forged at 523 K (250 °C), we move on to consider the Orowan mechanisms; the initial dislocation density prior to annealing was quantified as high as $3.0 \times 10^{16}/\text{m}^2$, whereas after annealing it decreased as low as $1.5 \times 10^{16}/\text{m}^2$. Subsequent quantification of dislocation density and the influence of dislocation substructure is the topic of ongoing research. Figure 13 shows representative HRTEM images and the corresponding FFT images before and after annealing. Hosford^[16] and others described dispersion (Orowan) strengthening of metals as a mechanism occurring when hard particles on slip planes form barriers to dislocation motion.^[29,33] Dislocations are expected to do one of two things during deformation: (1) bow around hard particles or (2) cut through soft particles. We primarily consider the first case (commonly known as Orowan strengthening) because from a thermodynamic perspective, our particles are anticipated to be hard oxides and nitrides based on chemical analysis and starting with

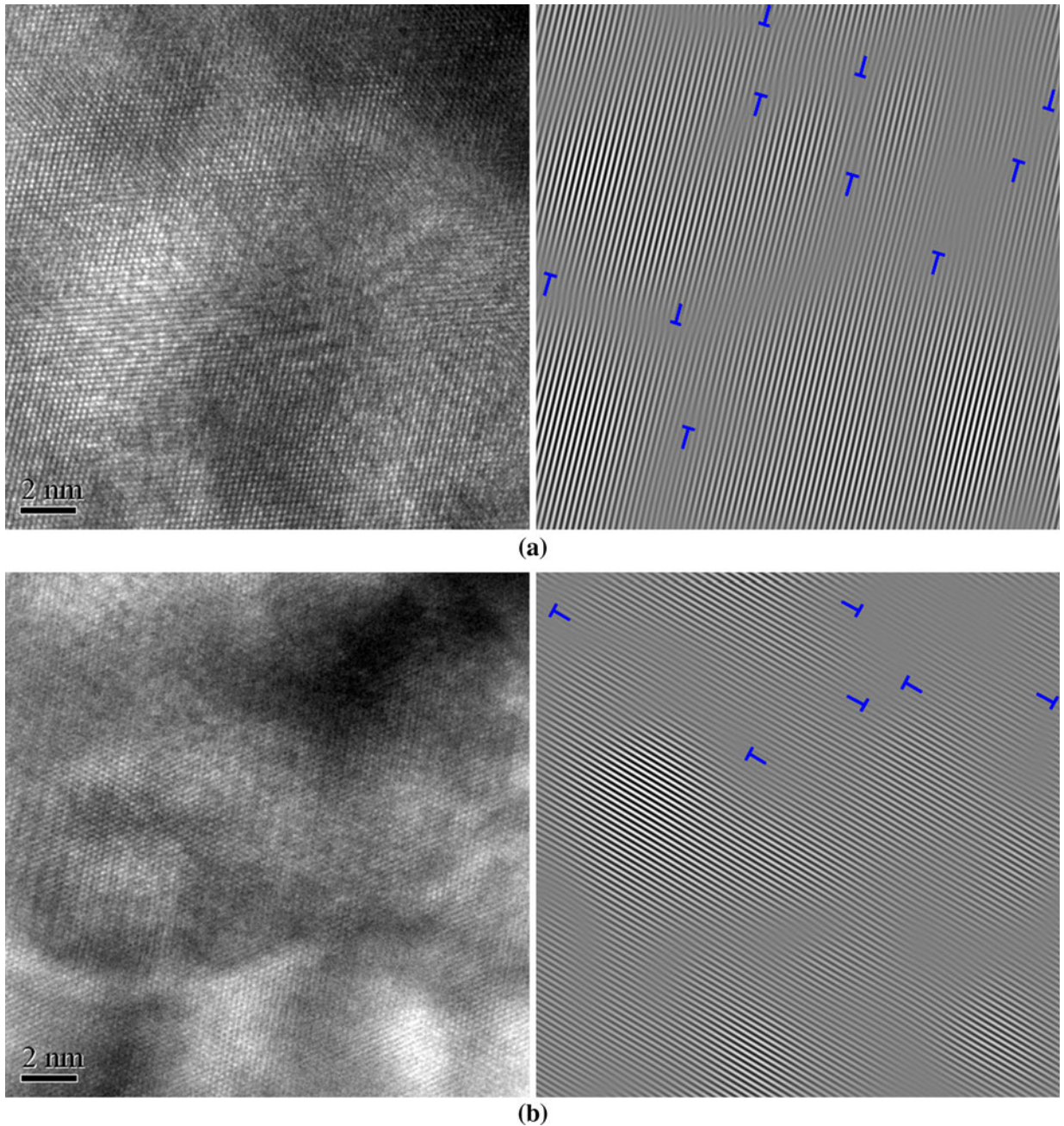


Fig. 13—Representative HRTEM images and corresponding FFT for cryomilled plate forged at 523 K (250 °C) (a) before annealing and (b) after annealing at 688 K (415 °C) for 10 min.

cryomilled AA 5083 powder.^[6,24] Recalling early research in this field, researchers investigated ball-milled alloys for their dispersion strengthening promise.^[34–36] Cryomilling was used later by researchers at Exxon to reduce grain size to obtain UFG microstructures in softer materials, like aluminum.^[37] The presence of oxides and nitrides in cryomilled aluminum is supported by an accumulating set of data in the literature, including, but not limited to, the work of Li *et al.*,^[6] Aikin *et al.*,^[38] Hayes *et al.*,^[39] and Sussegg.^[40] For now, we are simply refining the methods of Han *et al.*^[17] by adding the grain size relationship described herewith.^[17]

In his manuscript, he uses Eq. [3] to estimate the Orowan strengthening.

$$\sigma_{Or} = M \frac{0.4Gb}{\pi(1-\nu)^{1/2}} \frac{\ln(\bar{d}/b)}{\bar{\lambda}} \quad [3]$$

Equation [3] uses the orientation factor $M = 3.06$ for face-centered cubic aluminum, G is the shear modulus, b is the Burgers vector, ν is Poisson's ratio, and $\bar{d} = \sqrt{2/3} \cdot d$ and $\bar{\lambda} = \bar{d}(\sqrt{\pi/4f} - 1)$ are the mean dispersoid size and inter-particle distance, respectively.^[41,42] Han goes on to estimate a volume fraction

of dispersoids in a cryomilled Al-Mg alloy to be approximately 0.5 pct. Based on his assumptions, the Orowan strengthening in the alloy is 123 MPa.

To combine Han's method with our Hall-Petch analysis, we redefine σ_o in Eq. [4] as

$$\sigma_o = \sigma_{Or} + \sigma_{SS} \quad [4]$$

where we use $\sigma_o \sim 192$ MPa, determined from our linear fit in Figure 10. Using Han's approximation, the value we determined for σ_{Or} (~123 MPa), and the linear fit in Figure 10, it follows that the portion of σ_o attributable to σ_{SS} in our Hall-Petch curve is ~69 MPa. Comparing the estimates we use for Orowan and solid solution strengthening with the values of 55 MPa and 90 MPa that Huskins *et al.*^[22] give for the conventional AA 5083 H131 (work-hardened) system, which we accept here as the baseline, our estimates are within 55 pct and 23 pct of Huskins' values. If we take the yield strength of conventional, coarse-grained AA 5083 in the annealed condition (138 MPa, Table II), $\sigma_{SS} = \sigma_o$ in Eq. [4] (for the conventional AA 5083) and is ~138 MPa because there is negligible Orowan strengthening in the annealed conventional AA 5083. This value differs even more from Huskins' value. This disparity might be understood by reasoning that dispersoids and inclusions contribute little strengthening to the conventional material, which is considered a solid-solution-strengthened alloy. In fact, alloy AA 5083 contains more magnesium than the solubility limit indicated by the equilibrium phase diagram, as well as other alloying elements, including manganese, iron, and chromium. As discussed previously, these additions can precipitate and form dispersoids, acting as Orowan contributors.^[24,26,43] Thus, care must be taken in the interpretation of the data from conventional AA 5083 as an approach to isolate the Orowan mechanism during analysis of the cryomilled material's behavior. The increase in Orowan strengthening in our analysis *vs* Huskins *et al.*'s provides evidence to support the likelihood of nitrides and oxides contributing to the strength of the cryomilled material, likely in the form of ultrafine and nanometric inclusions.^[6]

A thorough discussion requires consideration of the difference in grain boundary orientation, HAB *vs* LAB. The results in Figure 8 indicate a large difference in HAB fraction between the conventional plate and cryomilled, forged plate—23 pct HAB and 77 pct

HAB, respectively. A high proportion of HAB reportedly can lead to grain boundary sliding (GBS) and even superplasticity in fine-grain materials at high temperatures.^[44,45] Because the change in dislocation density is relatively small (Figure 13) in the forged plate [523 K (250 °C)], in the annealed and as-received conditions, the GBS mechanism may be activated during forging, and we may cause a transition between the competing mechanisms of GBS and dislocation motion when forging at this temperature, which is approximately 0.42 T_m . This finding is consistent with literature data indicating that in the regime of 0.4 to 0.6 T_m , grain boundary diffusion is considered the controlling mechanism for superplastic flow.^[45] Alternatively, other researchers reported a possible lack of grain boundary mobility in cryomilled aluminum alloys where grain boundaries tend to be decorated with dispersion particles,^[46,47] which contradicts the notion that superplasticity can be induced in this case. A more complete study of grain boundary orientation in the UFG cryomilled materials is ongoing to clarify this issue.

To complete our analysis for this study, we consider the different contributions to strengthening, which are presented as a linear combination in Eq. [1]. The Hall-Petch strengthening for the plate forged at 523 K (250 °C) was calculated to be ~284 MPa, and Han's approximation together with our linear fit resulted in an estimate of σ_{Or} ~123 MPa and σ_{SS} ~69 MPa, respectively. Finally, the annealing data lead to an estimate of σ_p ~51 MPa, which is the difference in the yield strength before (521 MPa) and after annealing (470 MPa) the plate forged at 523 K (250 °C). These values sum to 527 MPa, which differs by 1.2 pct from the data presented in Table II. Subsequent calculations were performed for the other plates, and results are presented in Table III.

Figure 14 summarizes each strengthening contribution for the three cryomilled plates in the form of a bar chart.

B. Tensile Deformation

An examination of the stress-strain curves in Figure 9 reveals a consistent trend in the tensile response from the annealed, conventional AA 5083 through the cryomilled alloys forged at 723 K, 623 K, and 523 K (450 °C, 350 °C, and 250 °C). Aluminum alloys in the 5000 series are typically considered to be work hardenable,^[26] and

Table III. Summary of Measured Yield Strength Compared with Estimated Contributions and Totals

Material	Processing	Grain Size	Actual 0.2 pct YS (MPa)	Estimated				
				σ_{SS} (MPa)	σ_{OR} (MPa)	σ_p (MPa)	σ_{HP} (MPa)	σ_{Tot} (MPa)
UFG AA 5083	forged at 523 K (250 °C)	194 nm	521	69	123	51	284	527
	forged at 623 K (350 °C)	259 nm	451	69	123	0	246	438
	forged at 723 K (450 °C)	337 nm	400	69	123	0	215	407

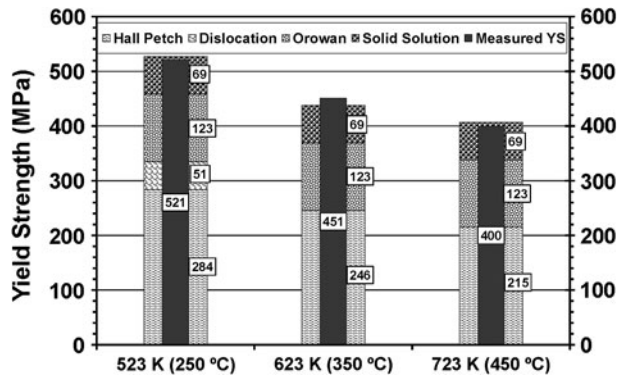


Fig. 14—Bar chart comparing predicted and actual strength of cryo-milled and forged plates.

significant interactions take place among the dislocations, dispersoids, and solute atoms, even after yielding. This quality in Al-Mg alloys and others is commonly referred to as the Portevin–Le Châtelier (PLC) effect.^[17,48–50] Han attributed the nature of the serrated flow of the stress–strain curve in three steps: (1) interactions of mobile dislocations with alloying elements (Mg, Mn, Cr, and Fe), (2) deformation twinning, and (3) detachment of dislocations from fine dispersoids (oxides and nitrides). Although deformation twins have been observed in cryomilled aluminum,^[20,51] we do not intend to focus on that aspect as a mechanism contributing to the PLC behavior. Considering the decrease in PLC serration in the stress–strain curves presented, dislocation interaction is the most likely explanation. Clearly, the PLC effect diminished as working temperature and grain size decreased, providing evidence that reduced dislocation mobility leads to reduced dynamic strain aging or PLC effect in tension.

In addition to the changes in PLC serrations, the representative curves in Figure 9 show notable differences in both prenecking and postnecking behavior, which also point to changes in dislocation activity^[52,53] in the materials produced and tested. The curves for the three UFG materials exhibited three distinctly different shapes (in addition to the PLC effect discussed already) with regard to work hardening, uniform elongation, and postnecking strain softening. A clear change was observed as work hardening, as well as uniform elongation, obviously decreases with decreasing grain size (and forging temperature). We also witnessed an apparent increase in the strain softening of the alloys in the postnecking region of the stress–strain curves. We have not completely characterized the differences in the stress–strain curves presented in this study, but ongoing investigations of these materials are attempting to correlate the grain size and morphology to these apparent changes. Using the available tensile data, a quantification of the strain hardening behavior of the three plates is presented in Figure 15, correlating the work-hardening rate with the true plastic strain for the materials forged at all three temperatures, including the annealed piece. By following the methods of other researchers such as Rodriguez *et al.*^[54] and Vogt *et al.*,^[55] we use Eq. [5]

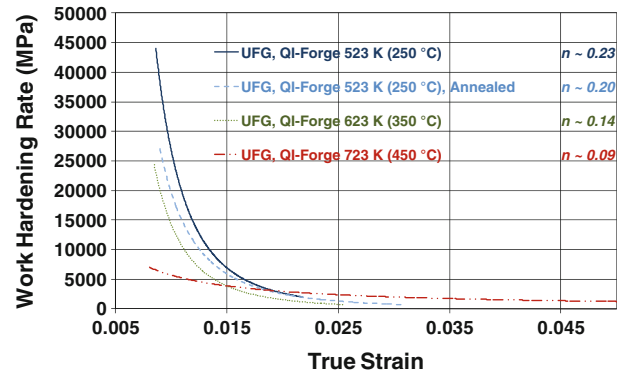


Fig. 15—Correlation of work-hardening rate θ to plastic strain, with corresponding strain hardening coefficients n for each plate shown on the plot.

$$\theta = \frac{d\sigma}{d\varepsilon} \quad [5]$$

where θ is the work-hardening rate. By plotting points from Eq. [5] vs the true strain, we show the material behavior over a range of strains. Strain-hardening behavior was also evaluated mathematically by fitting data in the plastic regime, before the UTS, to Eq. [6]

$$\sigma = K\varepsilon^n \quad [6]$$

where n is the strain-hardening exponent. Additionally, the strain-hardening exponent n is included on the plot in Figure 15, where all exponents were derived from a power law fit to data from true strains of 0.01 to 0.02. The work-hardening rate is initially higher for the as-forged 523 K (250 °C) forged plate vs the annealed plate and decreases with increasing forging temperature (and grain size), suggesting that dislocation strengthening is occurring more rapidly with more limited length scales. Although the mechanisms at work are not fully understood, the plot in Figure 15 shows convergences of the work-hardening rate that may be associated with the grain size associated with that particular level of strain during the tensile test. One possible explanation is stress-assisted grain boundary migration during the tensile test.^[56,57] Witkin *et al.*^[4] studied microstructural coarsening during thermomechanical processing and found that recovery or recrystallization occurred quickly after the onset of deformation, but it was not particularly sensitive to the strain rate.

V. CONCLUSIONS

Cryomilling is an effective means of generating initially nanocrystalline microstructures, although the grain structures tend to coarsen during consolidation and thermomechanical processing. This coarsening, however, is controllable and to some extent desirable, as it restores partially some of the ductility and toughness inherent in conventionally processed alloys. By maintaining fixed forging loads and cryomilling parameters, while varying forging temperatures, we

showed the ability to control grain growth and tailor properties of a bulk nanostructured Al-Mg alloy, specifically 5083 aluminum.

A chemical analysis and TEM observation showed the following:

1. The presence of fine dispersoids, some of which are likely in the form of inclusion particles of oxides and nitrides
2. Some dislocation accumulation in low temperature forgings [523 K (250 °C)].

We demonstrate that even in the UFG alloy dislocations are active mechanisms, both before and after yielding in tension. We present evidence pointing to the presence of oxides and nitrides in cryomilled aluminum to add to an accumulating set of data in the literature.

EBSD experiments showed a much greater ratio of HAB to LAB in the cryomilled, forged plate compared with the conventionally processed plate. A higher proportion of HAB could explain the relatively small increase in dislocations observed in annealed and as-received plates, supporting the contention that GBS contributed to deformation in the plate forged at 523 K (250 °C). A subsequent EBSD study of the plates forged at 623 K and 723 K (350 °C and 450 °C) is necessary to elucidate the contributions of the two deformation mechanisms—GBS and dislocation accumulation—during forging at different temperatures.

A Hall-Petch relationship has been demonstrated that is consistent with mechanical behavior for fine-grained alloys reported elsewhere. The test data are correlated with strength values predicted from the developed equations, but an improved treatment of the solid solution and Orowan mechanisms in the 5083 alloy may be necessary, especially to improve our understanding of the exact contribution to strength from oxygen and nitrogen presumed to exist in the form of oxides and nitrides.

ACKNOWLEDGMENTS

The authors gratefully acknowledge funding from The Office of Naval Research (Contract No. N00014-03-C0163) to produce and characterize the materials with the assistance of Dr. Piers Newbery. Also acknowledged is the Materials Design Institute, a joint research program between Los Alamos National Laboratory, LLC (LANS) and the College of Engineering, University of California–Davis (LANS Subcontract 25110-002-06) for funding to continue basic scientific research on the materials after they were produced. Mark R. van den Bergh and Cory A. Smith of DWA Aluminum Composites (Chatsworth, CA) are acknowledged for their technical expertise and manufacturing assistance during cryomilling. Henry (Mic) Meeks and Mark Fleming of Advance Materials & Manufacturing Technologies (Granite Bay, CA) are acknowledged for their technical advice and expertise during quasi-isostatic forging.

REFERENCES

1. Z.H. Zhang, B.Q. Han, K.H. Chung, and E.J. Lavernia: *Metall. Mater. Trans. A*, 2006, vol. 37A, pp. 2265–73.
2. D.B. Witkin and E.J. Lavernia: *Progr. Mater. Sci.*, 2006, vol. 51 (1), pp. 1–60.
3. F.A. Mohamed: *Acta Mater.*, 2003, vol. 51 (14), pp. 4107–19.
4. D. Witkin, B.Q. Han, and E.J. Lavernia: *J. Mater. Res.*, 2005, vol. 20 (8), pp. 2117–26.
5. A.P. Newbery, S.R. Nutt, and E.J. Lavernia: *JOM*, 2006, vol. 58 (4), pp. 56–61.
6. Y. Li, W. Liu, V. Ortolan, W.F. Li, Z. Zhang, R. Vogt, N.D. Browning, E.J. Lavernia, and J.M. Schoenung: *Acta Mater.*, 2010, vol. 58 (5), pp. 1732–40.
7. T.J. Van Daam and C. Clifford: US Patent 7344675, The Boeing Company, Chicago, IL.
8. A.P. Newbery, B. Ahn, T.D. Topping, P.S. Pao, S.R. Nutt, and E.J. Lavernia: *J. Mater. Process. Tech.*, 2008, vol. 203 (1–3), pp. 37–45.
9. D. Witkin, B.Q. Han, and E.J. Lavernia: *Metall. Mater. Trans. A*, 2006, vol. 37A, pp. 185–94.
10. ANSI H35.1-2004, Alloy And Temper Designation Systems For Aluminum.
11. J.B. Cohen: *Practical Organic Chemistry*, Macmillan, London, UK, 1910, p. 356.
12. ASTM, “Standard Test Methods for Determining Average Grain Size,” 2004.
13. ASTM, “Standard Test Methods for Tension Testing of Metallic Materials,” 2008.
14. T.D. Topping, E.J. Lavernia, M. Kuruvilla, and T.S. Srivatsan: *The Cyclic Fatigue, Damage Initiation, Propagation and Fracture Behavior of Cryomilled Aluminum Alloy 5083: Influence of Secondary Processing*, Ed. M.A. Inman, Wiley, New York, NY, 2010.
15. T.D. Topping, Z. Zhang, E.J. Lavernia, T.S. Srivatsan, and M. Kuruvilla: *Processing and Fabrication of Advanced Materials XIX*, Ed. R.J.L.D. Bhattacharyya and T.S. Srivatsan, University of Auckland Press, Auckland, New Zealand, 2011, pp. 21–34.
16. W.F. Hosford: *Mechanical Behavior of Materials*, Cambridge University Press, New York, NY, 2005, pp. 188–206.
17. B.Q. Han, F.A. Mohamed, and E.J. Lavernia: *J. Mater. Sci.*, 2003, vol. 38 (15), pp. 3319–24.
18. B. Ahn, R. Mitra, E.J. Lavernia, and S.R. Nutt: *J. Mater. Sci.*, 2010, vol. 45 (17), pp. 4790–95.
19. F. Shen, J. Zhou, Y. Liu, R. Zhu, S. Zhang, and Y. Wang: *Comput. Mater. Sci.*, 2010, vol. 49 (2), pp. 226–35.
20. Y.T. Zhu: *J. Mater. Eng. Perform.*, 2005, vol. 14 (4), pp. 467–72.
21. T. Shanmugasundaram, M. Heilmaier, B.S. Murty, and V.S. Sarma: *Mater. Sci. Eng. A*, 2010, vol. 527 (29–30), pp. 7821–25.
22. E.L. Huskins, B. Cao, and K.T. Ramesh: *Mater. Sci. Eng. A*, 2010, vol. 527 (6), pp. 1292–98.
23. Y. Li, Y.H. Zhao, V. Ortolan, W. Liu, Z.H. Zhang, R.G. Vogt, N.D. Browning, E.J. Lavernia, and J.M. Schoenung: *Mater. Sci. Eng. A*, 2009, vol. 527 (1–2), pp. 305–16.
24. V.L. Tellkamp, A. Melmed, and E.J. Lavernia: *Metall. Mater. Trans. A*, 2001, vol. 32A, pp. 2335–43.
25. *Metals Handbook, Properties and Selection: Nonferrous Alloys and Special Purpose Materials*, 10th ed., vol. 2, ASM, Materials Park, OH, 1990.
26. ASM Handbooks Online: *Properties and Selection: Nonferrous Alloys and Special-Purpose Materials, Properties of Wrought Aluminum and Aluminum Alloys*, vol. 2, 2002.
27. N.J. Petch: *J. Iron Steel Inst.*, 1953, vol. 25 (1), pp. 25–28.
28. E.O. Hall: *Proc. Phys. Soc. Lond. Sect. B*, 1951, vol. 64 (381), pp. 747–53.
29. M.A. Meyers and K.K. Chawla: *Mechanical Behavior of Materials*, 1999, Prentice Hall, Upper Saddle River, NJ, pp. 247–81.
30. R.W. Hayes, D. Witkin, F. Zhou, and E.J. Lavernia: *Acta Mater.*, 2004, vol. 52 (14), pp. 4259–71.
31. A. Forcellese and F. Gabrielli: *Int. J. Mach. Tools Manufact.*, 2000, vol. 40 (9), pp. 1285–97.
32. O. Jensrud and K. Pedersen: *J. Mater. Process. Tech.*, 1998, vols. 80–81, pp. 156–60.
33. G.E. Dieter: *Metallurgy and Metallurgy Engineering Series*, McGraw-Hill, New York, NY, 1961, pp. 118–45.
34. G.S. Ansell: *Acta Metall.*, 1961, vol. 9 (5), pp. 518–19.
35. J.E. White: *J. Met.*, 1965, vol. 17 (6), p. 587.

36. N. Hansen: *Acta Metall.*, 1970, vol. 18 (1), p. 137.
37. R. Petkovic-Luton and J. Vallone: U.S. Patent 4619699, to Exxon Research and Engineering Company, 1986.
38. B.J.M. Aikin, R.M. Dickerson, D.T. Jayne, S. Farmer, and J.D. Whittenberger: *Scripta Metall. Mater.*, 1994, vol. 30 (1), pp. 119–22.
39. R.W. Hayes, P.B. Berbon, and R.S. Mishra: *Metall. Mater. Trans. A*, 2004, vol. 35A, pp. 3855–61.
40. O. Susegg: *Micron Microscop. Acta*, 1992, vol. 23 (1–2), pp. 223–24.
41. B.Q. Han and D.C. Dunand: *Mater. Sci. Eng. A*, 2000, vol. 277 (1–2), pp. 297–304.
42. A. Kelly and R. Nicholson: *Strengthening Methods in Crystals*, Elsevier, New York, NY, 1971, p. 629.
43. ASM Handbooks Online, *Alloy Phase Diagrams, Al Binary Alloy Phase Diagrams*, Al-Mg. ASM International, vol. 3, 2002.
44. J.C. Huang, I.C. Hsiao, T.D. Wang, and B.Y. Lou: *Scripta Mater.*, 2000, vol. 43 (3), pp. 213–20.
45. O.D. Sherby and J. Wadsworth: *Progr. Mater. Sci.*, 1989, vol. 33 (3), pp. 169–221.
46. I. Roy, M. Chauhan, F.A. Mohamed, and E.J. Lavernia: *Metall. Mater. Trans. A*, 2006, vol. 37A, pp. 721–30.
47. V.L. Tellkamp, E.J. Lavernia, and A. Melmed: *J. Mater. Res.*, 2001, vol. 16 (4), pp. 938–44.
48. H. Tensi and H. Ehrhardt: *Zeitschrift Fur Metallkunde*, 1968, 59, no. 3.
49. M. Abbadi, P. Hahner, and A. Zeghloul: *Mater. Sci. Eng. A*, 2002, vol. 337 (1–2), pp. 194–201.
50. J.Z. Chen, L. Zhen, L. Fan, S. Yang, S. Dai, and W. Shao: *Transactions of Nonferrous Metals Society of China*, 2009, vol. 19 (5), pp. 1071–75.
51. B. Li, B.Y. Cao, K.T. Ramesha, and E. Ma: *Acta Mater.*, 2009, vol. 57 (15), pp. 4500–07.
52. Y.H. Zhao, Y.Z. Guob, Q. Wei, T.D. Topping, A.M. Dangelewicz, Y.T. Zhu, T.G. Langdon, and E.J. Lavernia: *Mater. Sci. Eng. A*, 2009, vol. 525 (1–2), pp. 68–77.
53. F. Tang and J.M. Schoenung: *Mater. Sci. Eng. A*, 2008, vol. 493 (1–2), pp. 101–03.
54. R. Rodriguez, R.W. Hayes, P.B. Berbon, and E.J. Lavernia: *Acta Mater.*, 2003, vol. 51 (4), pp. 911–29.
55. R.G. Vogt, Z. Zhang, T.D. Topping, E.J. Lavernia, and J.M. Schoenung: *J. Mater. Process. Tech.*, 2009, vol. 209 (11), pp. 5046–53.
56. M. Jin, A.M. Minor, E.A. Stach, and J.W. Morris, Jr.: *Acta Mater.*, 2004, vol. 52 (18), pp. 5381–87.
57. D.S. Gianola, S. van Petegem, M. Legros, S. Brandstetter, H. Van Swygenhoven, and K.J. Hemker: *Acta Mater.*, 2006, vol. 54 (8), pp. 2253–63.